Constraints on Spin-Dependent Short-Range Interaction between Nucleons

K. Tullney,[1,*] F. Allmendinger,[2] M. Burghoff,[3] W. Heil,[1] S. Karpuk,[1] W. Kilian,[3] S. Knappe-Grüneberg,[3]
W. Müller,[3] U. Schmidt,[2] A. Schnabel,[3] F. Seifert,[3] Yu. Sobolev,[1,†] and L. Trahms[3]

[1]*Institut für Physik, Johannes Gutenberg-Universität, 55099 Mainz, Germany*
[2]*Physikalisches Institut, Universität Heidelberg, 69120 Heidelberg, Germany*
[3]*Physikalisch-Technische Bundesanstalt Berlin, 10587 Berlin, Germany*
(Received 27 March 2013; published 3 September 2013)

We search for a spin-dependent P- and T-violating nucleon-nucleon interaction mediated by light pseudoscalar bosons such as axions or axionlike particles. We employ an ultrasensitive low-field magnetometer based on the detection of free precession of colocated ^{3}He and ^{129}Xe nuclear spins using SQUIDs as low-noise magnetic flux detectors. The precession frequency shift in the presence of an unpolarized mass was measured to determine the coupling of pseudoscalar particles to the spin of the bound neutron. For boson masses between 2 and 500 μeV (force ranges between 3×10^{-4} m and 10^{-1} m) we improved the laboratory upper bounds by up to 4 orders of magnitude.

Axions are light, pseudoscalar particles that arise in theories in which the Peccei-Quinn $U(1)$ symmetry has been introduced to solve the strong CP problem [1]. They could have been created in early stages of the Universe being attractive candidates to the cold dark matter that could compose up to $\sim 1/3$ of the ingredients of the Universe [2]. Several constraints from astrophysics, cosmology, and laboratory experiments have been applied in order to prove or rule out the existence of the axion, i.e., constrain the axion's mass m_a and/or its couplings. The mass range, in which axions are still likely to exist, could thus be narrowed down to a window reaching from μeV [3] up to some meV [4] (axion window).

Most axion searches look for the conversion of an axion of galactic [5], solar [6], or laboratory [7] origin into a photon in the presence of a static magnetic field. However, any axion or axionlike particle that couples with both scalar and pseudoscalar vertices to fundamental fermions would also mediate a parity and time-reversal symmetry-violating force between a fermion f and the spin of another fermion f_σ, which is parametrized by a Yukawa-type potential with range λ and a monopole-dipole coupling given by [8]

$$V_{\rm sp}(\vec{r}) = \frac{\hbar^2 g_s^f g_p^{f_\sigma}}{8\pi m_{f_\sigma}}(\vec{\sigma} \cdot \hat{r})\left(\frac{1}{\lambda r} + \frac{1}{r^2}\right)e^{-r/\lambda}, \qquad (1)$$

where $\vec{\sigma}$ is the spin vector and λ is the range of the Yukawa force with $\lambda = \hbar/(m_a c)$. Thus, the entire axion window can be probed by searching for spin-dependent short-range forces in the range between 20 μm and 0.2 m. g_s^f and $g_p^{f_\sigma}$ are dimensionless scalar and pseudoscalar coupling constants which in our case correspond to the scalar coupling of an axionlike particle to a nucleon ($g_s^f = g_s^N$) and its pseudoscalar coupling to a polarized bound neutron ($g_p^{f_\sigma} = g_p^n$). Accordingly, we have $m_{f_\sigma} = m_n$. $\hat{r}$ is the

unit distance vector from the bound neutron to the nucleon. The potential given by Eq. (1) effectively acts near the surface of a massive unpolarized sample as a pseudomagnetic field and gives rise to a shift $\Delta\nu_{\rm sp} = 2V_\Sigma/h$, e.g., in the precession frequency of nuclear spin-polarized gases (^{3}He and ^{129}Xe), which according to the Schmidt model [9] can be regarded as an effective probe of spin-polarized bound neutrons. The potential V_Σ is obtained by integration of $V_{\rm sp}(r)$ from Eq. (1) over the volume of the massive unpolarized sample averaged over the volume of the polarized spin sample, each having a cylindrical shape. Based on the analytical derivation of $V_{\Sigma,\infty}$ for disk-shaped spin and matter samples with respective thicknesses D and d [10], we obtain

$$V_\Sigma = V_{\Sigma,\infty}\,\eta(\lambda)$$
$$= 2\pi N\kappa\frac{\lambda^2}{D}e^{-\Delta x/\lambda}(1 - e^{-D/\lambda})(1 - e^{-d/\lambda})\eta(\lambda). \quad (2)$$

$\eta(\lambda)$ takes account for the finite size in transverse direction of our cylindrical samples and Δx represents the finite gap between them. Furthermore, $\kappa = \hbar^2 g_s^N g_p^n/(8\pi m_n)$ and N is the nucleon number density of the unpolarized matter sample. $\eta(\lambda)$ is determined numerically for our cylindrically shaped spin and matter samples at "close" position (see Fig. 1). [$\eta(\lambda)$ can be expressed reasonably well by the fit function $\eta_{\rm fit}(\lambda) = (1 + 27.8\lambda^{1.34})/(1 + 234\lambda^{1.31})$.]

Our experimental approach to search for nonmagnetic, spin-dependent interactions is to use an ultrasensitive low-field comagnetometer based on detection of free spin precession of gaseous, nuclear polarized samples [11]. The Larmor frequencies of ^{3}He and ^{129}Xe in a guiding magnetic field B are given by $\omega_{\rm L,He(Xe)} = \gamma_{\rm He(Xe)}B$, with $\gamma_{\rm He(Xe)}$ being the gyromagnetic ratios of the respective gas species [12,13], with $\gamma_{\rm He}/\gamma_{\rm Xe} = 2.754\,081\,59(20)$. The influence of the ambient magnetic field and its temporal
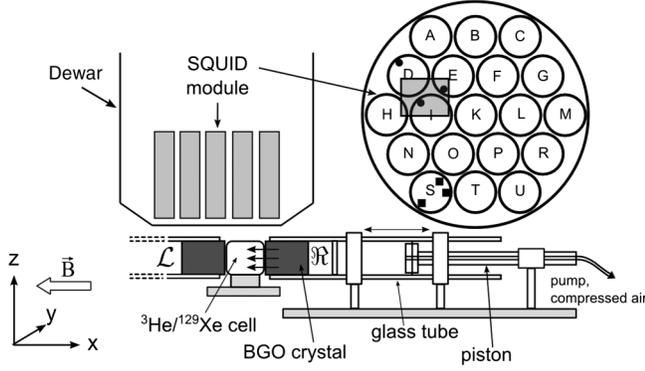
FIG. 1. Sketch of experimental setup. The lower plane SQUIDs in module D, E, and I marked as (●) are used to detect the ^{3}He/^{129}Xe free spin precession. The center of the cylindrical spin sample cell ($D = 60$ mm, $\oslash_D = 58$ mm) has an average distance of $\bar{z} = 66$ mm to the sensors. The relative position of the cell in the projection onto the (x, y) plane is indicated by the gray square. SQUIDs in module S marked as (■) are used for the gradiometric sensor arrangements. The unpolarized mass (cylindrical BGO crystal: $d = 70$ mm, $\oslash_d = 60$ mm) can be moved along the x axis (B-field axis) to "close" ($\Delta x_c = 2.2$ mm) and "distant" ($\Delta x_d = 170$ mm) positions and vice versa (see text). This is accomplished by a piston driven glass tube with the BGO fixed at its cell-facing side. The two measuring arrangements "left" ($\mathcal{L}$) and "right" ($\mathfrak{R}$) are shown.

fluctuations cancels in the difference of measured Larmor frequencies of the colocated spin samples

$$\Delta\omega = \omega_{\text{He}} - \frac{\gamma_{\text{He}}}{\gamma_{\text{Xe}}}\omega_{\text{Xe}}. \quad (3)$$

On closer inspection, a resulting constant frequency shift $\Delta\omega_{\text{lin}}$, e.g., due to Earth's rotation, is not compensated by comagnetometry. That is discussed in [14], together with frequency shifts due to the generalized Ramsey-Bloch-Siegert shift. The latter ones are directly proportional to the particular net magnetization $A_{\text{He(Xe)}}e^{-t/T^*_{2,\text{He(Xe)}}}$ and also are included in the weighted frequency difference $\Delta\omega(t)$:

$$\Delta\omega(t) = \Delta\omega_{\text{lin}} + \epsilon_{\text{He}}A_{\text{He}}e^{-t/T^*_{2,\text{He}}} - \epsilon_{\text{Xe}}A_{\text{Xe}} \cdot e^{-t/T^*_{2,\text{Xe}}}. \quad (4)$$

Accordingly, its equivalent, the weighted phase difference $\Delta\Phi(t) = \Phi_{\text{He}}(t) - (\gamma_{\text{He}}/\gamma_{\text{Xe}})\Phi_{\text{Xe}}(t)$, is sensitive to a phase drift given by

$$\Delta\Phi(t) = \Phi_0 + \Delta\omega_{\text{lin}}t - \epsilon_{\text{He}}T^*_{2,\text{He}}A_{\text{He}}e^{-t/T^*_{2,\text{He}}}$$
$$+ \epsilon_{\text{Xe}}T^*_{2,\text{Xe}}A_{\text{Xe}}e^{-t/T^*_{2,\text{Xe}}}. \quad (5)$$

Because of the knowledge of these side effects, any anomalous frequency shifts generated by nonmagnetic spin interactions, such as the quested short-range interaction, can be analyzed by looking at $\Delta\omega(t)$ and $\Delta\Phi(t)$, respectively. A sudden frequency change $\Delta\omega_{\text{sp}}$ stemming from the pseudoscalar Yukawa potential $V_{\text{sp}}(r)$ would occur at an

instant $t = t_0$, e.g., by moving a massive matter sample close to the precessing nuclei. This would lead to an additional linear phase drift $\Delta\omega_{\text{sp}}t$ in Eq. (5) for $t > t_0$. For further analysis, it is useful to develop Eq. (5) in a Taylor expansion of 5th order around t_0 (the criterion to use a Taylor expansion up to the 5th order was that the reduced $\chi^2/$d.o.f. of the fit equals 1). The weighted phase difference $\Delta\Phi(t)$ can then be described by

$$\Delta\Phi(t') = a + b(t')t' + ct'^2 + dt'^3 + et'^4 + ft'^5, \quad (6)$$

with $t' = t - t_0$. The coefficient of the linear term now reads

$$b(t') = \Delta\omega_{\text{lin}} + \Delta\omega^w_{\text{sp}}(t') + \epsilon_{\text{He}}A'_{\text{He}} - \epsilon_{\text{Xe}}A'_{\text{Xe}}. \quad (7)$$

Note that $\Delta\omega^w_{\text{sp}}(t') = 2\pi\Delta\nu^w_{\text{sp}}\Theta(\pm t')$ is the only time-dependent term in Eq. (7), so that a change $\delta b = b_c - b_d = 2\pi\Delta\nu^w_{\text{sp}}$ of $b(t')$ at $t = t_0$ would directly indicate the existence of the short-range interaction. [($\pm$) in the argument of the Heaviside step function has to be set ($-$) for the sequence $c \rightarrow d$ and ($+$) for the reverse one, $d \rightarrow c$. Furthermore, for runs $j = 1, 2, 3$ the BGO was moved at $t_0 = 8700$ s, otherwise at $t_0 = 10\,800$ s.] With our special choice of $t' = t - t_0$, the linear coefficient of the Taylor expansion does not depend on T^*_2 and thus is insensitive to possible changes in T^*_2. The impact of the T^*_2 dependence of higher order terms on the determination of $b(t')$ is discussed in detail in the section on systematic uncertainties.

The experiments were performed inside the magnetically shielded room BMSR-2 at the Physikalisch-Technische Bundesanstalt Berlin (PTB) [15]. A homogeneous guiding magnetic field of about 350 nT was provided inside the shielded room by means of a square coil pair (B_x coils) of edge length 1800 mm. A second square coil pair (B_y coils) arranged perpendicular to the B_x coils was used to manipulate the sample spins, e.g., $\pi/2$ spin flip by nonadiabatic switching [11]. The major components of the experimental setup within BMSR-2 are shown in Fig. 1. For the detection of spin precession we used a multichannel low-T_c dc-SQUID device [16,17]. The ^{3}He/^{129}Xe nuclear spins were polarized outside the shielding by means of optical pumping. Low-relaxation cylindrical glass cells (GE180) were filled with the polarized gases and placed directly beneath the Dewar as close as possible to the SQUID sensors. The SQUID sensors detect a sinusoidal change in magnetic flux due to the nuclear spin precession of the gas atoms. In order to obtain a high common mode rejection ratio, three first order gradiometric sensor combinations were used in order to suppress environmental disturbance fields such as vibrational modes. Figure 1 shows their positions with respect to each other and with respect to the ^{3}He/^{129}Xe sample cell. The system noise of the SQUID gradiometer configurations was between 3 and 10 fT/$\sqrt{\text{Hz}}$ in the range of the ^{3}He/^{129}Xe spin-precession frequencies, i.e., $4 < \nu_L < 12$ Hz, while typical signal amplitudes reached

10 pT for helium and 3 pT for xenon at the beginning of the spin-precession cycle.

Typically, the optimum conditions in terms of long transverse relaxation times (T_2^*) and high SNR were met at a gas mixture with pressures of ^{3}He:Xe($91\%^{129}$Xe):$N_2 \approx (2:8:35)$ mbar. Nitrogen was added to suppress spin-rotation coupling in bound Xe-Xe van der Waals molecules [18,19]. As unpolarized matter sample we used a cylindrical BGO crystal ($Bi_4Ge_3O_{12}$, $\rho = 7.13$ g/cm^3). BGO has a high nucleon number density, is a nonconductive material that shows low Johnson-Nyquist noise, and is said to have an unusual magnetism-related behavior in weak constant magnetic fields ($\chi_{mag} \approx 0$ ppm) [20–22]. For systematic checks, the BGO crystal could be placed left ($\mathcal{L}$) and right ($\mathfrak{R}$) with respect to the ^{3}He/^{129}Xe sample cell (see Fig. 1). Since $V_{sp}(\vec{r}) \propto \vec{\sigma} \cdot \hat{r}$, $\Delta\nu_{sp}$ changes its sign in going from $\mathcal{L}$ to $\mathfrak{R}$. This has to be considered by averaging the $\mathcal{L}$ and $\mathfrak{R}$ results. On the other hand, $\Delta\nu_{sp}$ drops out averaging $\mathcal{L}$ and $\mathfrak{R}$ without sign change. In case of a nonzero spin-dependent axion fermion interaction, a shift $\Delta\nu_{sp}^w$ in the weighted frequency difference [Eq. (3)] can be extracted from respective frequency measurements in "close" and "distant" positions given by

$$\Delta\nu_{sp}^w = \frac{2V_\Sigma^c}{h}\left(1 - \frac{\gamma_{He}}{\gamma_{Xe}}\right), \tag{8}$$

assuming $V_{\Sigma,He} = V_{\Sigma,Xe} = V_{\Sigma,n} \equiv V_\Sigma$ (Schmidt model) and $V_\Sigma^d \ll V_\Sigma^c$.

We performed 10 measurement runs lasting approximately 9 h each. For each measurement run, the BGO crystal was moved after $t_0 \approx 3$ h from close to distant position ($c \to d$) or vice versa ($d \to c$). The asymmetric timing takes account for the smaller SNR in the second measurement block due to the exponential damping (T_2^*) of the signal amplitude which was $T_{2,He}^* \approx 53$ h and $T_{2,Xe}^* \approx 5$ h, typically. By this measure, comparable statistics were obtained for both BGO positions.

As discussed in detail in [14], the data from each run were divided into sequential time intervals of $\tau = 3.2$ s. For each obtained subdata set, a χ^2 minimization was performed using an appropriate fit function to extract the phases ϕ_{He}, ϕ_{Xe} and the frequencies ω_{He}, ω_{Xe} with the corresponding errors. In a further step, the accumulated phase $\Phi_{He(Xe)}(t')$ was determined for each run in order to derive the weighted phase difference $\Delta\Phi(t')$. Then, Eq. (6) was fitted simultaneously to the data set $\Delta\Phi(t')$ that was determined for the three gradiometers of each measurement run. From the resulting fit parameters $\bar{a}$, $\bar{b}_c$, $\bar{b}_d$, $\bar{c}$, $\bar{d}$, $\bar{e}$, $\bar{f}$ and by use of Eqs. (7) and (8), the frequency shift $\overline{\Delta\nu}_{sp}$ is then extracted from

$$\overline{\Delta\nu}_{sp} = \frac{\bar{b}_c - \bar{b}_d}{2\pi\left(1 - \frac{\gamma_{He}}{\gamma_{Xe}}\right)}. \tag{9}$$

For six runs (2, 3, 4, 5, 9, 10), the BGO crystal was positioned at $\mathcal{L}$, otherwise at $\mathfrak{R}$. For all $\mathcal{L}$ runs, the results were multiplied by (-1): $\overline{\Delta\nu}_{sp} = -\overline{\Delta\nu}_{sp,\mathcal{L}}$. In Fig. 2(a), values $\overline{\Delta\nu}_{sp}$ for the individual runs are shown together with their correlated 1σ errors. [The correlated errors are calculated as the square root of the diagonal elements of the covariance matrix of the least χ^2 fit model of Eq. (6) with the proper statistical weights. The uncorrelated errors are about a factor of 30 smaller and not included in the error bars shown in Fig. 2.] From the calculation of the weighted mean, one gets $\overline{\overline{\Delta\nu}}_{sp} = (-2.9 \pm 2.3)$ nHz. As a consistency check, we reanalyzed our 2009 data, where we looked for a possible Lorentz-violating (LV) sidereal frequency modulation [14]. Since no mass was moved, $\bar{b}_c = \bar{b}_d$ should hold, using the fit function of Eq. (6) and a hypothetical time $t_0 = 10\,800$ s. Figure 2(b) shows the results $\overline{\Delta\nu}_{check}$ for all 7 measurement runs together with their correlated 1σ errors. The weighted mean of the LV data gives $\overline{\overline{\Delta\nu}}_{check} = (-1.4 \pm 3.4)$ nHz. The χ^2/d.o.f. of the data to their respective weighted means ($\overline{\overline{\Delta\nu}}_{sp}$, $\overline{\overline{\Delta\nu}}_{check}$) gives 2.29 and 2.38, indicating that the errors on the measured frequency shifts (Fig. 2) are somewhat underestimated. In order to take this into account, the errors are scaled to obtain a χ^2/d.o.f. of one, as recommended, e.g., by [23,24].

At the 95% C.L., our results for the measured frequency shifts are

$$\overline{\overline{\Delta\nu}}_{sp} = (-2.9 \pm 6.9)\ \text{nHz}, \tag{10}$$

$$\overline{\overline{\Delta\nu}}_{check} = (-1.4 \pm 10.5)\ \text{nHz}, \tag{11}$$

indicating that (i) we find no evidence for a pseudoscalar short-range interaction mediated by axionlike particles and

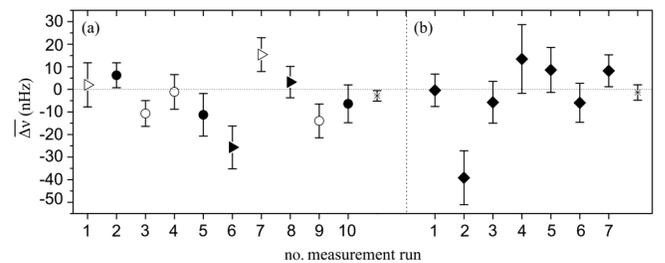

FIG. 2. (a) Extracted frequency shifts $\overline{\Delta\nu}_{sp}$ (with correlated 1σ error) of the 10 measurement runs. The triangles specify the $\mathfrak{R}$, the circles the $\mathcal{L}$ arrangement of the BGO crystal. Full symbols indicate the $c \to d$ sequence, hollow symbols the opposite case ($d \to c$). (b) Results $\overline{\Delta\nu}_{check}$ obtained from the LV data using the same fit model [Eq. (6)]. Since no mass was moved, we expect no shift in the spin precession frequency. The rightmost symbols in both plots (stars) indicate the respective weighted means (1σ error).

(ii) the cross-check analysis of our LV data is compatible with zero within the error bars, as expected.

Discussion of systematic uncertainties.—The movement of the BGO crystal can produce correlated effects that may mimic a pseudoscalar frequency shift or even compensate the effect we are looking for. Two effects caused by a nonzero magnetic susceptibility of the BGO have to be considered, by taking $\chi_{\text{mag}} = -19$ ppm, which is the high-field limit ($B > 0.1$ T) [21]. (a) The BGO at the close position slightly changes the magnetic field across the volume of the ^{3}He/^{129}Xe sample cell. This effect drops out to first order due to comagnetometry. To second order, however, the difference in their molar masses leads to a difference (Δz) in their center of masses (barometric formula), which is $\Delta z = 1.2 \times 10^{-7}$ m for our cylindrical sample cell. This results in a frequency shift of $\Delta\nu_{\text{sys}} = \Delta z |\langle \partial B/\partial z \rangle|_{\text{ind}} \gamma_{\text{He}}/2\pi \leq 0.03$ nHz for induced field gradients in the vertical direction of $|\langle \partial B/\partial z \rangle|_{\text{ind}} \leq 0.08$ pT/cm. The field gradients were calculated using COMSOL MULTIPHYSICS, a finite element analysis software. Compared to the measured frequency shift [Eq. (10)], this systematic effect is negligible. (b) More serious is the fact that a change of the magnetic field gradient by the BGO also influences the T_2^* times of ^{3}He and ^{129}Xe. The direct approach is to extract T_2^* and thus ΔT_2^* via the exponential decay of the signal amplitudes with the BGO in close and distant positions. The most accurate distinction between $(T_2^*)_c$ and $(T_2^*)_d$ was obtained through a fit to the amplitude ratio $A_{\text{Xe}}(t')/A_{\text{He}}(t')$ given by $f_{\text{fit}}(t') = We^{-t'/T_{\text{eff}}^*}$ with $T_{\text{eff}}^* = T_{2,\text{He}}^* T_{2,\text{He}}^*/(T_{2,\text{He}}^* - T_{2,\text{He}}^*)$. According to [11,25,26], a relation between $\Delta T_{2,\text{He}}^*$, $\Delta T_{2,\text{Xe}}^*$, and ΔT_{eff}^* can be derived

$$\frac{\Delta T_{\text{eff}}^*}{(T_{\text{eff}}^*)^2} = -\frac{\Delta T_{2,\text{He}}^*}{(T_{2,\text{He}}^*)^2} + \frac{\Delta T_{2,\text{He}}^*}{(T_{2,\text{Xe}}^*)^2} \approx -0.5 \frac{\Delta T_{2,\text{He}}^*}{(T_{2,\text{He}}^*)^2} \quad (12)$$

by taking the respective diffusion coefficients of ^{3}He and ^{129}Xe in the gas mixture and using the approximation $\varnothing_D/2 = D/2 \approx R = 30$ mm for our cylindrically shaped cell. We obtain an upper limit of $|\Delta T_{2,\text{He}}^*| < 160$ s for a possible T_2^* change. From that the systematic frequency shift $\Delta\nu_{\text{sys}}^{T_2^*}$ on $b(t')$ due to the higher order terms of Eq. (6) can be estimated to be

$$\left| \Delta\nu_{\text{sys}}^{T_2^*} \right| \leq \left| \frac{\frac{\Delta T_{2,\text{He}}^*}{(T_{2,\text{He}}^*)^2}\left(\frac{E_{\text{He}}'}{T_{2,\text{He}}^*} - \frac{1}{2}\frac{E_{\text{Xe}}'}{T_{2,\text{Xe}}^*}\right)\frac{t_0}{2}}{2\pi(1 - \gamma_{\text{He}}/\gamma_{\text{Xe}})} \right| \approx 0.1 \text{ nHz}. \quad (13)$$

Here we used Eq. (9), replacing $\bar{b}_c$ and $\bar{b}_d$ by the temporal means $2\bar{c}_c \langle t' \rangle_{t'}$ and $2\bar{c}_d \langle t' \rangle_{t'}$ of the quadratic term in Eq. (6) with $\bar{c}_{c(d)} = \{-(E_{\text{He}}'/2)/(T_{2,\text{He}}^*)^2 + (E_{\text{Xe}}'/2)/(T_{2,\text{Xe}}^*)^2\}_{c(d)}$ and $E_{\text{He(Xe)}}' = \epsilon_{\text{He(Xe)}} A_{\text{He(Xe)}}' T_{2,\text{He(Xe)}}^*$. Values for the respective $E_{\text{He(Xe)}}'$ phase amplitudes were extracted from the fit function [Eq. (6)] applied to the data
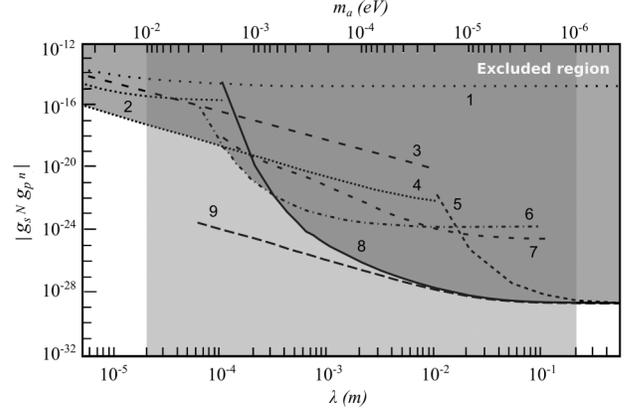

FIG. 3. The experimental 95% confidence upper limit on $|g_s^N g_p^n|$ plotted versus λ, the range of the Yukawa force with $\lambda = \hbar/(m_a c)$. The axion window is indicated by the light gray area. (1) result of [28], (2) result of [29], (3) result of [30], (4) result of [31], (5) result of [32], (6) result of [33], (7) result of [34], (8) this experiment ($\Delta x = 2.2$ mm) [35], (9) expected results for $\Delta x \approx 0$ mm using the same data set demonstrates the gain in measurement sensitivity for $\lambda < 10^{-3}$ m. See [36] for bounds on the pseudoscalar short-range force between polarized electrons and unpolarized nucleons. Raffelt [37] points out that much tighter constraints on $|g_s^N g_p^n|$ can be inferred by combining constraints on g_s from stellar energy-loss arguments and g_p from searches for anomalous monopole-monopole forces.

and result to be $\langle E_{\text{He}}' \rangle = 11.5$ rad and $\langle E_{\text{Xe}}' \rangle = 0.1$ rad. Finally, $\langle t' \rangle_{t'}$ was taken to be $\langle t' \rangle_{t'} \approx t_0/2$.

From Eq. (13) a conservative estimate of the systematic error can be made with $|\Delta\nu_{\text{sys}}^{T_2^*}| = \pm 0.2$ nHz (95% C.L.), which brings us to the final result

$$\overline{\overline{\Delta\nu}}_{\text{sp}} = (-2.9 \pm 6.9 \pm 0.2) \text{ nHz} \qquad (95\% \text{ C.L.}) \quad (14)$$

for the measured pseudoscalar frequency shift.

From the total error $\delta(\overline{\overline{\Delta\nu}}_{\text{sp}}) = \pm 7.1$ nHz, we can then derive exclusion bounds for $|g_s^N g_p^n|$ using Eq. (2) and $|\delta(\overline{\overline{\Delta\nu}}_{\text{sp}})| \geq 2V_{\Sigma}^c/h$, which are shown in Fig. 3.

We have substantially improved the bounds on a spin-dependent short-range interaction between polarized (bound) neutrons and unpolarized nucleons over most of the axion window, tightening existing constrains on axion-like particles heavier than 20 μeV by up to 4 orders of magnitudes.

And there are clear strategies on how to improve our experimental sensitivity. (i) Close contact of the spin system with the matter sample. For $\Delta x \approx 0$ mm, our present measurement sensitivity will significantly increase for $\lambda < 10^{-3}$ m (see Fig. 3). (ii) Moving the spin-matter sample more frequently between its set positions ($c \leftrightarrow d$ and/or $\mathcal{L} \leftrightarrow \mathfrak{R}$). This results in a different time structure for the linear term in the fit model of Eq. (6) such that the correlated error approaches the uncorrelated one. This was already demonstrated in [14]. (iii) Magnetic susceptibility related

*Corresponding author.
tullnek@uni-mainz.de
†On leave from PNPI, St. Petersburg, Russia.

[1] R. D. Peccei and H. R. Quinn, Phys. Rev. Lett. **38**, 1440 (1977).
[2] J. Jaeckel and A. Ringwald, Annu. Rev. Nucl. Part. Sci. **60**, 405 (2010).
[3] S. Asztalos *et al.*, Phys. Rev. D **69**, 011101(R) (2004).
[4] G. G. Raffelt, Annu. Rev. Nucl. Part. Sci. **49**, 163 (1999).
[5] S. Asztalos *et al.*, Phys. Rev. Lett. **104**, 041301 (2010).
[6] E. Arik *et al.*, J. Cosmol. Astropart. Phys. 02 (2009) 008.
[7] K. Ehret *et al.*, Phys. Lett. B **689**, 149 (2010).
[8] J. E. Moody and F. Wilczek, Phys. Rev. D **30**, 130 (1984).
[9] Th. Schmidt, Z. Phys. **106**, 358 (1937).
[10] O. Zimmer, Phys. Lett. B **685**, 38 (2010).
[11] C. Gemmel *et al.*, Eur. Phys. J. D **57**, 303 (2010).
[12] M. Pfeffer and O. Lutz, J. Magn. Reson., Ser. A **108**, 106 (1994).
[13] http://www.codata.org.
[14] C. Gemmel *et al.*, Phys. Rev. D **82**, 111901 (2010).
[15] J. Bork *et al.*, in *Proceedings of Biomag. 2000: The 12th International Conference on Biomagnetism, Espoo, Finland, 2000* (Helsinki University of Technology, Espoo, Finland, 2000), p. 970.
[16] D. Drung, Physica (Amsterdam) **368C**, 134 (2002).
[17] M. Burghoff, S. Hartwig, W. Kilian, A. Vorwerk, and L. Trahms, IEEE Trans. Appl. Supercond. **17**, 846 (2007).
[18] B. Chann, I. A. Nelson, L. W. Anderson, B. Driehuys, and T. G. Walker, Phys. Rev. Lett. **88**, 113201 (2002).
[19] B. C. Anger, G. Schrank, A. Schoeck, K. A. Butler, M. S. Solum, R. J. Pugmire, and B. Saam, Phys. Rev. A **78**, 043406 (2008).
[20] E. A. Kravchenko, V. G. Orlov, and M. P. Shlykov, Russ. Chem. Rev. **75**, 77 (2006).
[21] S. Yamamoto, K. Kuroda, and M. Senda, IEEE Trans. Nucl. Sci. **50**, 1683 (2003).
[22] B. C. Grabmaier and R. Oberschmid, Phys. Status Solidi (a) **96**, 199 (1986).
[23] Particle Data Group, Phys. Lett. B **592**, 11 (2004).
[24] W. H. Press, S. A. Tenkolsky, W. T. Vetterling, and B. P. Flannery, *Numerical Recipes: The Art of Scientific Computing* (Cambridge University Press, New York, 2007), 3rd ed.
[25] G. D. Cates, S. R. Schaefer, and W. Happer, Phys. Rev. A **37**, 2877 (1988).
[26] W. Kilian, A. Haller, F. Seifert, D. Grosenick, and H. Rinneberg, Eur. Phys. J. D **42**, 197 (2007).
[27] R. Kc, Y. N. Gowda, D. Djukovic, I. D. Henry, G. H. J. Park, and D. Raftery, J. Magn. Reson. **205**, 63 (2010).
[28] S. Baeßler, V. V. Nesvizhevsky, K. V. Protasov, and A. Yu. Voronin, Phys. Rev. D **75**, 075006 (2007).
[29] T. Jenke *et al.*, arXiv:1208.3875v1.
[30] A. P. Serebrov *et al.*, JETP Lett. **91**, 6 (2010).
[31] A. K. Petukhov, G. Pignol, D. Jullien, and K. H. Andersen, Phys. Rev. Lett. **105**, 170401 (2010).
[32] A. N. Youdin, D. Krause, Jr., K. Jagannathan, L. R. Hunter, and S. K. Lamoreaux, Phys. Rev. Lett. **77**, 2170 (1996).
[33] M. Bulatowicz, R. Griffith, M. Larsen, J. Mirijanian, C. B. Fu, E. Smith, W. M. Snow, H. Yan, and T. G. Walker, preceding Letter, Phys. Rev. Lett. **111**, 102001 (2013).
[34] P.-H. Chu *et al.*, Phys. Rev. D **87**, 011105(R) (2013).
[35] See A. G. Glenday, C. E. Cramer, D. F. Phillips, and R. L. Walsworth, Phys. Rev. Lett. **101**, 261801 (2008) for a discussion on theoretical calculations of the neutron spin contribution to the nuclear angular momentum in ^{3}He ($I = 1/2$) and ^{129}Xe ($I = 1/2$) (approximatively 87% and 75%). This refinement of nuclear model that goes beyond the Schmidt model used in [31,32,34] of Fig. 3 increases our upper bounds by a factor of 1.4.
[36] S. A. Hoedel, F. Fleischer, E. G. Adelberger, and B. R. Heckel, Phys. Rev. Lett. **106**, 041801 (2011).
[37] G. G. Raffelt, Phys. Rev. D **86**, 015001 (2012).